2004-09

Microstructural modification of as-cast NiAl bronze by friction stir processing

Oh-Ishi, Keiichiro; McNelley, Terry R.

K. Oh-Ishi, T.R. McNelley, "Microstructural modification of as-cast NiAl bronze by friction stir processing," Metallurgical and Materials Transactions A, v.35A, (September 2004), pp. 2951-2961.
http://hdl.handle.net/10945/55376

Microstructural Modification of As-Cast NiAl Bronze by Friction Stir Processing

KEIICHIRO OH-ISHI and TERRY R. McNELLEY

The application of friction stir processing (FSP) to a cast NiAl bronze (NAB) material is presented as a means for selective modification of the near-surface layers by converting as-cast microstructures to a wrought condition in the absence of macroscopic shape change. This may enable selective surface hardening of cast components. The complex physical metallurgy of the NAB is reviewed, and microstructure changes associated with FSP for a selected set of processing parameters are examined by optical microscopy (OM) and transmission electron microscopy (TEM) methods. Direct temperature measurement in the stir zone is infeasible and, so, these microstructure changes are used to estimate peak temperatures in the stir zone. The persistence of a Fe_3Al phase (κ_{II}) indicates that peak temperatures are below the solvus for this phase, while the presence of transformation products of the β phase, including fine Widmanstätten α, bainite, and martensite, indicates that peak temperatures exceed the eutectoid temperature for the reaction $\beta \rightarrow \alpha + \kappa_{III}$ throughout the stir zone.

I. INTRODUCTION

FRICTION stir processing (FSP) is an emerging metalworking technology that can provide localized modification and control of microstructures in near-surface layers of processed metallic components.[1,2,3] This technology represents an adaptation of the principles of friction stir welding, a solid-state joining process originally developed at The Welding Institute.[4] In FSP, a cylindrical, wear-resistant tool consisting of a smaller-diameter pin with a concentric, larger-diameter shoulder is rotated and forced into the surface of a single piece of material. The rotating tool penetrates until the shoulder comes into contact with the workpiece surface. Then, the tool is traversed along a path on the surface, as illustrated in Figure 1, in a single- or multipass process. The tool depicted in Figure 1 has spiral threads, and tool designs involving stepped or fluted pins have also been employed.[1] The tool shoulder acts to constrain upward metal flow caused by insertion of the pin, and metal flow in the workpiece may include vertical (parallel to the tool axis) as well as horizontal (in the plane of tool rotation) components (Figure 1).

Upon initial insertion of the rotating tool, friction between the tool and the surface of the material results in heating and a "stirring" action that, in turn, produces adiabatic heating and local softening of the material. A processed zone, or stir zone, is produced by severe plastic deformation with movement of material about the pin. The combination of very large deformations and adiabatic heating results in microstructure refinement and homogenization, leading to improved strength and ductility of material in the stir zone.[1–3,5–10] The FSP may also result in closure of porosity and inclusion redistribution in castings and, thereby, contribute to improved mechanical properties. Microstructure refinement and homogenization may also have a beneficial effect on corrosion resistance. In effect, FSP of a cast metal may result in conversion of the as-cast microstructure to a wrought condition in the absence of macroscopic shape change and, thereby, provide a means for modification of surface layers and surface hardening of cast components.

During FSP, the severe straining as well as steep gradients in strain, strain rate, and temperature make direct measurement of temperature within the stir zone infeasible. Nevertheless, analysis of the effect of FSP on microstructure may provide insight into the thermomechanical history of material in and nearby the stir zone when coupled with alloy-constitution and phase-relationship data. This article is a report of an investigation into the effects of FSP on the microstructure of an as-cast NiAl bronze (NAB) material for the purpose of assessing the thermomechanical history of various locations within the stir zone.

The NAB alloys are widely used for marine components due to their good combination of corrosion resistance, strength, fracture toughness, friction coefficients, and nonsparking behavior.[11] Many cast components produced in NAB involve thick sections, and the resulting slow cooling rates contribute to coarse microstructures and reduced physical and mechanical properties.[12] In such applications, the NAB materials may not be heat treatable and, so, FSP represents an alternative means of selectively strengthening the surfaces of such components.

The addition of nickel and iron to copper-aluminum alloys extends the terminal fcc α-phase field and suppresses the γ-phase formation that occurs in binary Cu-Al alloys.[13,14,15] The γ phase forms by the eutectoid reaction $\beta \rightarrow \alpha + \gamma$ in binary alloys containing more than 9.5 wt pct Al;[16] the γ corrodes preferentially due to its high Al content and, so, its presence is deleterious.[13,17] The Ni and Fe additions have also been found to increase NAB mechanical properties through the precipitation of complex κ phases in both the α and the β.[15] Thus, NABs are copper-based quaternary alloys; the alloy of interest in the present work (UNS95800) is nominally Cu-9Al-5Ni-4Fe (compositions in wt pct).[18]

KEIICHIRO OH-ISHI, Postdoctoral Research Associate, and TERRY R. McNELLEY, Professor of Materials Science, are with the Department of Mechanical and Astronautical Engineering, Naval Postgraduate School, Monterey, CA 93943-5146. Contact e-mail: tmcnelley@nps.edu

Manuscript submitted January 7, 2004.

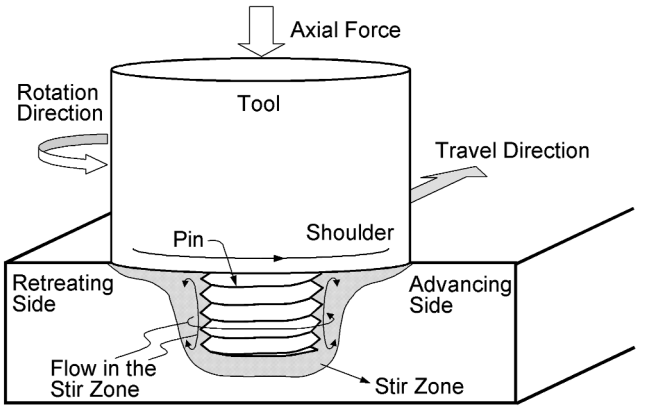

Fig. 1—A schematic of FSP illustrates severe plastic deformation in the vicinity of the tool pin.

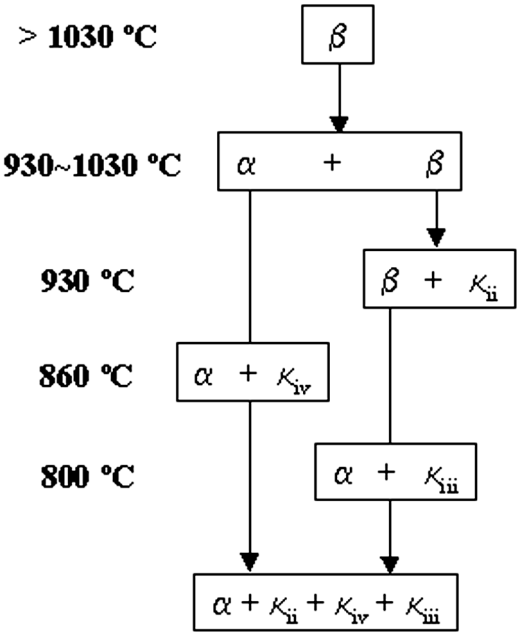

(*a*)

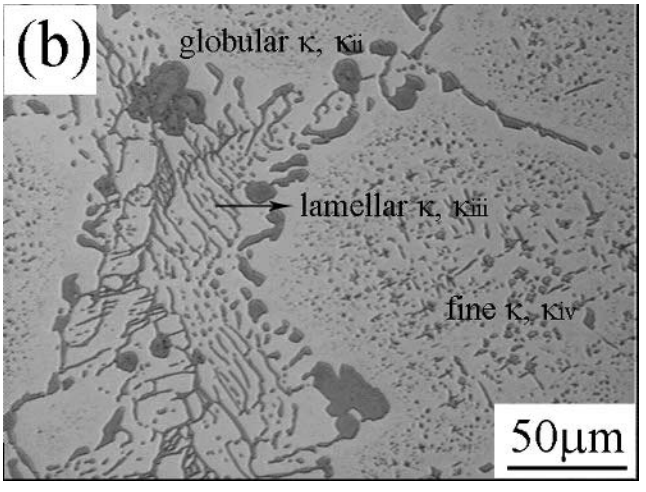

Fig. 2—(*a*) A schematic indicates the sequence of transformations during equilibrium cooling of a Cu-9Al-5Ni-4Fe alloy.[13–15,17,19–27] (*b*) A typical as-cast microstructure for near-equilibrium cooling of the alloy.

The constitution and transformation characteristics of NAB materials have been described in detail elsewhere.[13–15,17,19–27] An as-cast Cu-9Al-5Ni-4Fe alloy solidifies as a single-phase β solid solution, and the sequence of transformations during equilibrium cooling is summarized in Figure 2(a). The micrograph of Figure 2(b) was obtained from a cast NAB component that required 10 days to cool to room temperature, corresponding to a nominal cooling rate of $\sim 10^{-3}$ °C s^{-1}, and is assumed to represent an equilibrium microstructure. The as-cast alloy remains fully β until cooling to about 1030 °C. Below this temperature, primary α phase forms in the β with a Widmanstätten morphology, followed by nucleation of globular κ, which is nominally Fe_3Al, in the β, beginning at 930 °C. The globular morphology is apparent in the micrograph of Figure 2(b), and this phase is usually termed κ_{ii}. (In Cu-Al-Ni-Fe alloys containing ≥5 wt pct Fe, an Fe_3Al phase forms with a dendritic morphology and is termed κ_i.[22,24]) At about 860 °C, the solubility of Fe is exceeded in the α, and fine κ precipitates begin to form; these finer precipitates are also nominally Fe_3Al and are usually termed κ_{iv}. The remaining β decomposes by a eutectoid reaction at about 800 °C that results in the formation of a nickel-rich κ phase, κ_{iii}, which has a lamellar morphology. Proeutectoid κ_{iii} may exhibit a globular morphology.

The α phase is an fcc terminal solid solution having a lattice parameter of $a_0 = 0.364$ nm.[22] The Fe_3Al phases (κ_{ii} and κ_{iv}) have a DO_3 structure; the lattice parameter of κ_{ii} is 0.571 nm, while that of κ_{iv} is 0.577 nm.[22,24,26] The NiAl (κ_{iii}) phase exhibits a B2 structure with a lattice parameter of 0.288 nm.[22,24,25] Fully ordered Fe_3Al (κ_{ii} and κ_{iv}) and NiAl (κ_{iii}) phases will have interatom spacings that differ by less than 1 pct and are, therefore, difficult to distinguish by diffraction methods alone.

II. EXPERIMENTAL PROCEDURES

The material examined in this investigation conforms to the composition specification for UNS95800 NAB. The data are summarized in Table I. The FSP was accomplished at the Rockwell Scientific Company (Thousand Oaks, CA) using a tool having a shoulder diameter of 23.8 mm and pin diameter of 7.95 mm. The pin depth was 6.65 mm and the pin was machined with a spiral groove. In the present investigation, as-cast NAB material was processed in a modified milling machine using a tool rotation rate of 800 rpm, a traversing rate of 152 mm m^{-1} (6 in. m^{-1}), and with the tool axis inclined ~3 deg opposite the direction of tool advance.[28]

Optical microscopy (OM) involved standard sample preparation methods. Samples were etched in a two-step process involving, first, immersion for 1 to 2 seconds in a solution of 40 mL water −40 mL ammonium hydroxide −2 mL hydrogen peroxide (30 pct), rinsing in water, followed by immersion for 1 to 2 seconds in a solution of 60 mL water −30 mL phosphoric acid −10 mL hydrogen peroxide. Etched samples were examined using bright-field (BF) illumination in a Jenaphot 2000 apparatus equipped with a digital imaging system. Transmission electron microscopy (TEM) was accomplished with a Topcon 002B instrument operating at 200 kV. Samples for TEM examination were obtained by first sectioning with a low-speed diamond saw to obtain a transverse slice through the stir zone of processed material.

Table I. Composition Specifications[18] and Data for the UNS95800 NAB Alloy Examined in This Investigation

Element	Cu	Al	Ni	Fe	Mn	Si	Pb
Min-max	(min) 79.0	8.5 to 9.5	4.0 to 5.0	3.5 to 4.5	0.8 to 1.5	0.10 (max)	0.03 (max)
Nominal	81	9	5	4	1	—	—
Alloy	81.2	9.39	4.29	3.67	1.20	0.05	<0.005

Then, disks 3 mm in diameter and having normal directions parallel to the travel direction were thinned to perforation by electropolishing using a 33 pct nitric acid −67 pct methanol solution initially cooled to −25 °C; ion milling using an Hitachi E-300 ion mill operating at 4 kV for ~1 hour was employed with selected samples.

III. RESULTS

A. *Optical Microscopy*

Figure 3 is a montage of optical micrographs from a transverse section that contains the stir zone in material processed by FSP. The montage extends into the as-cast base metal. The direction of tool advance is into the page and, so, the advancing side (tangential, velocity at the tool surface is parallel to the travel direction) is to the right-hand side, while the retreating side (tangential velocity at the tool surface is antiparallel to the travel direction) is to the left-hand side. The stir zone is 23 to 24 mm in width and ~5 mm in depth. The machine compliance allows the axial force on the tool to displace it upward. This, as well as tool wear, results in a stir-zone depth that is less than the tool-pin length. The boundary between the stir zone and base metal is sharp on the advancing side and directly under the tool, but it is indistinct on the retreating side. Base-metal grains are distorted in a region nearby the boundary of the stir zone, although the sense of shearing varies from location to location along the boundary. Dark-etching features in this region may reflect partial reversion of the lamellar $\alpha + \kappa_{iii}$ to form β due to the heating associated with FSP, followed by rapid cooling as the tool advances. The region outside the stir zone that has experienced relatively small deformations and heating is often termed the thermomechanically affected zone (TMAZ).

Figure 4 consists of a series of higher-magnification optical micrographs representing regions along a vertical traverse through the center of the stir zone at the approximate locations indicated in Figure 3. Region 1 in Figures 3 and 4 is nearest the surface that is in contact with the tool shoulder and exhibits a refined structure, while region 2 is located further below the surface and exhibits bandlike features. Figure 5(a) shows the microstructure of region 1 at a still-higher magnification, and coarse (~20 μm), globular particles of κ_{ii} are evident to the left of center in this image. Two morphologies of the α-Cu phase, which is lightest-etching phase in this material, are also apparent. Most of the volume of the α is in grains that are roughly ellipsoidal in shape and elongated in a direction perpendicular to the axis of tool rotation. The dark-etching areas apparent at lower magnification (Figure 4, region 1) are now seen in Figure 5(a) to consist of Widmanstäten α as well as bainite and martensite (darkest features). Coarse globular κ_{ii} and the bandlike structure that is observed further below the surface in region 2 are also revealed at higher magnification in Figure 5(b). The light-etching α phase is again elongated in a direction perpendicular to the tool axis, and the dark-etching areas observed at lower magnification are now seen to consist of a combination of Widmanstätten α, bainite, and martensite.

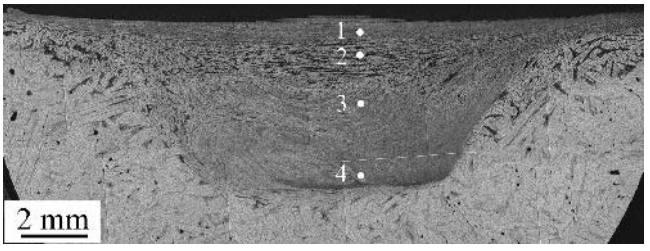

Fig. 3—A montage of optical micrographs from a transverse cross section shows the stir zone in the NAB material. The advancing side is to the right; the retreating side is to the left. The numbers indicate locations of the regions observed at higher magnification.

Globular κ_{ii} particles are evident in both regions 1 and 2. The volume fraction of the coarse, elongated α-Cu grains is greater, while the Widmanstätten α is finer in region 2 when compared to region 1. The lamellar structure associated with $\alpha + \kappa_{iii}$ is not apparent in any of these micrographs. Altogether, these observations suggest that the lamellar $\alpha + \kappa_{iii}$ present in as-cast material has reverted to β during the severe deformation and heating of FSP. However, the primary α formed during equilibrium cooling has not been completely retransformed to β and, so, the microstructure during FSP mainly consists of α and β in varying amounts, depending on the local peak temperature. Both phases deform and then the β transforms on subsequent cooling, giving Widmanstätten α, or bainite or martensite, depending on the cooling rates following passage of tool. Such cooling rates are expected to be on the order of 10^0 °C s^{-1}, *i.e.*, much faster than associated with equilibrium cooling. The transformation sequence of β under conditions of high cooling rates is summarized in Figure 5(c).[15]

Returning to the micrographs in Figure 4, region 3, located at the middle of the stir zone, shows fine and equiaxed grains when compared to region 1. This region exhibits dark-etching areas in locations between the α grains, but the amount of fine β transformation products is smaller than in region 2. Finally, region 4 is at the bottom of the stir zone; a grain-flow pattern is evident in the vicinity of the stir zone/TMAZ boundary, and the apparent grain size in this region is the finest in this stir zone.

B. *The TEM Results*

1. *Upper regions of the stir zone*

Figure 6 shows TEM micrographs for a location just below the surface on the advancing side from a location corresponding to region 2 in Figure 3 (*i.e.*, the banded region). A BF

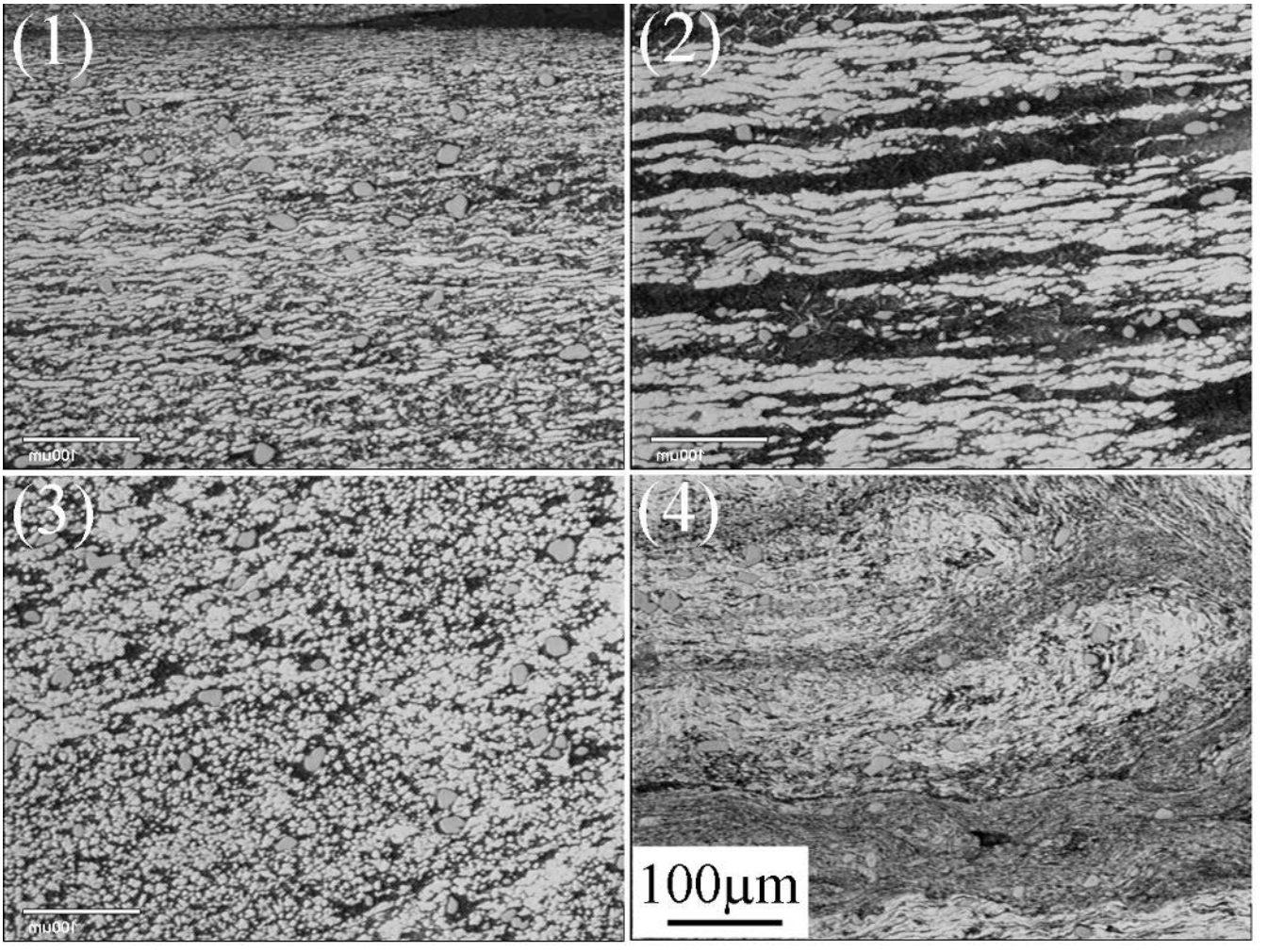

Fig. 4—Optical micrographs at higher magnification from regions 1 through 4, as indicated in Fig. 3. Light-etching areas are α phase; dark-etching areas are β transformation products that include Widmanstätten α, bainite, and martensite.

image is shown in Figure 6(a), and corresponding dark-field (DF) images at this position are shown in Figures 6(b) through (d); the DF images correspond, respectively, to the spots labeled B through D that are indicated on the selected-area diffraction (SAD) pattern inset in Figure 6(b). Fine globular precipitates and a very fine structure having a lamellar appearance are evident in Figures 6(a) and (b). An elongated, rod-like grain is apparent in Figure 6(c), which is α phase that has formed by a bainitic transformation from β phase during cooling. Figure 6(d) shows a martensite structure. The diffuse streaking along some directions in the SAD pattern reflects the large strains and presence of stacking faults that accompany the martensitic transformation at high cooling rates.

The fine-globular- and fine-lamellar-appearing precipitates, as well as the bainite and martensite, all indicate transformation at low temperatures under high cooling rates. It appears that fine globular particles precipitate initially. In the DF image, most of the precipitates have the same orientation in the matrix, despite residing in regions that comprise the other various transformation products. This indicates that precipitation of the globular phase occurs prior to the bainite or martensite transformations, or prior to the formation of the lamellar-appearing precipitates. Although the crystal structure of globular precipitates was not determined in this study, energy-dispersive spectrometry (EDS) analysis showed that these precipitates are an Fe-rich phase. Hasan, Lorimer, and Ridley[23] have documented the presence of such Fe-rich precipitates in a previous report. The Fe-rich precipitate had a B2 structure and formed along with martensite during quenching. By tempering at a low temperature (500 °C to 700 °C) after quenching, the martensite reverted to α and κ_{iii}, with the κ_{iii} phase precipitating on the pre-existing Fe-rich phase. In a separate study, Hasan, *et al.*[25] have also reported that such composite precipitates had a center consisting of an Fe-rich phase and an outer layer of the NiAl (κ_{iii}) phase. They confirmed by electron diffraction and EDS analysis that the Fe-rich phase was now Fe_3Al having the DO_3 structure. Thus, the globular particles observed in the present study are deemed to be an Fe-Al phase that has formed at low temperatures. For this reason, these particles do not correspond directly to the separate κ_{ii} and κ_{iv} precipitates that form at higher temperatures.

In addition, the lamellar-appearing structure is much finer than that in as-cast NAB and is similar to upper-bainite structures observed in ferrous alloys. The lamellar phase has a common orientation throughout regions such as that in Figure 6(a),

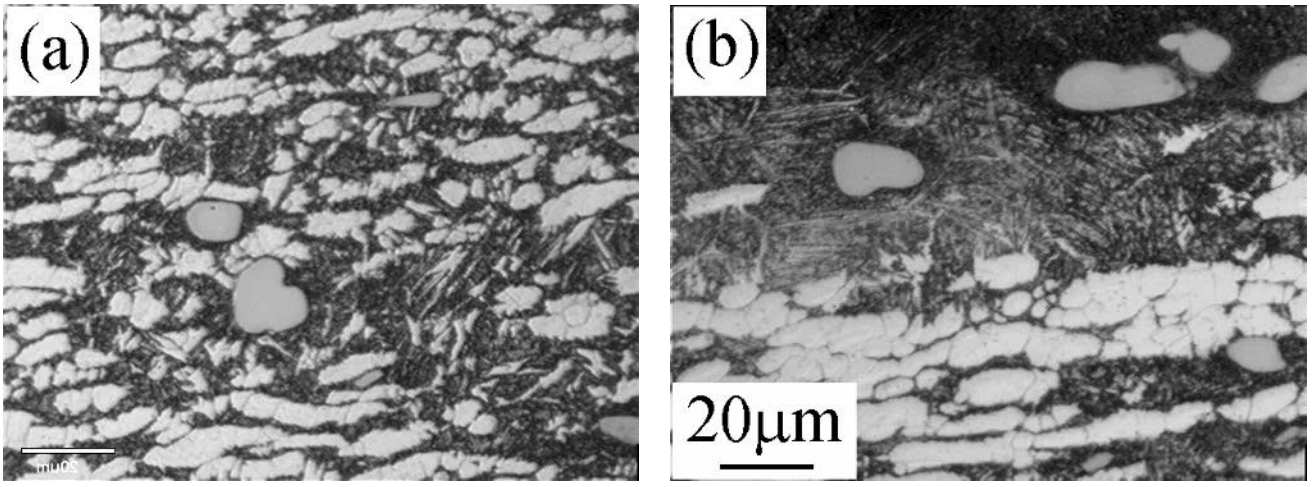

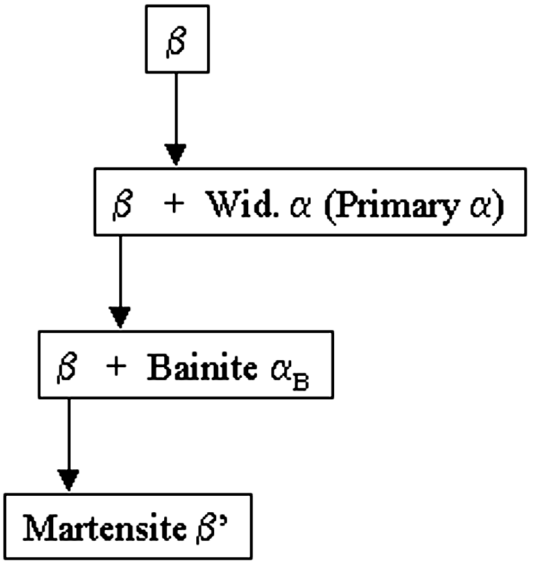

(*c*)

Fig. 5—High-magnification optical micrographs for (*a*) region 1, corresponding to a location nearest the surface; and (*b*) region 2, which is located further below the surface and exhibits a bandlike structure. (*c*) The transformation sequence is shown for β during cooling at higher rates such as experienced during FSP.

is separated by fine α phase, and is found in association with martensite, *e.g.* as in Figure 6. It is, therefore, deemed that these lamellar-appearing particles form by a bainite transformation at low temperatures. Following an initial diffusion-controlled transformation, the remaining β transforms to martensite, leading to such highly mixed microstructures.

Figure 7 is a BF TEM image of the α phase in region 2. The OM data in Figure 4 showed that region 2 comprised alternating, elongated light and dark bands and that the light bands are this α phase, while the dark bands are various transformation products of the β phase. In the α grains, individual dislocations, dislocation tangles, and subgrains are apparent, and the grain and subgrain boundaries appear to be irregularly curved. Such a structure reflects recrystallization followed by further deformation and recovery during the severe straining of the FSP.

2. *Midregions of the stir zone*

Figure 8 shows TEM micrographs obtained at region 3, near the center of the stir zone. Although the microstructure is not distinct in the BF image in Figure 8(a), both fine lamellar-appearing and fine globular particles are evident in the DF image in Figure 8(b), obtained using spot B in the SAD pattern, which is consistent with a B2-type structure. The spacing of lamella is, again, very much finer than that in the as-cast structure shown in Figure 2(b) and is comparable to the lamellar-appearing structure seen in the upper regions of the stir zone (Figure 6(b)).

Further analysis of this region is illustrated in Figure 9. This is another location in the same sample as that in Figure 8. This SAD pattern is consistent with a (100) pattern for a B2-type structure. The micrograph in Figure 9(b) was acquired with spot B in the SAD pattern and highlights both lamellar and globular particles. In contrast, Figure 9(c) was obtained from the streak denoted C and highlights plates aligned along the (110) plane. Such plates reflect a variant of a martensitic transformation product. Thus, martensite is still observed along with bainite in this region, and the formation of these transformation products is not suppressed despite the lower cooling rates anticipated in locations further

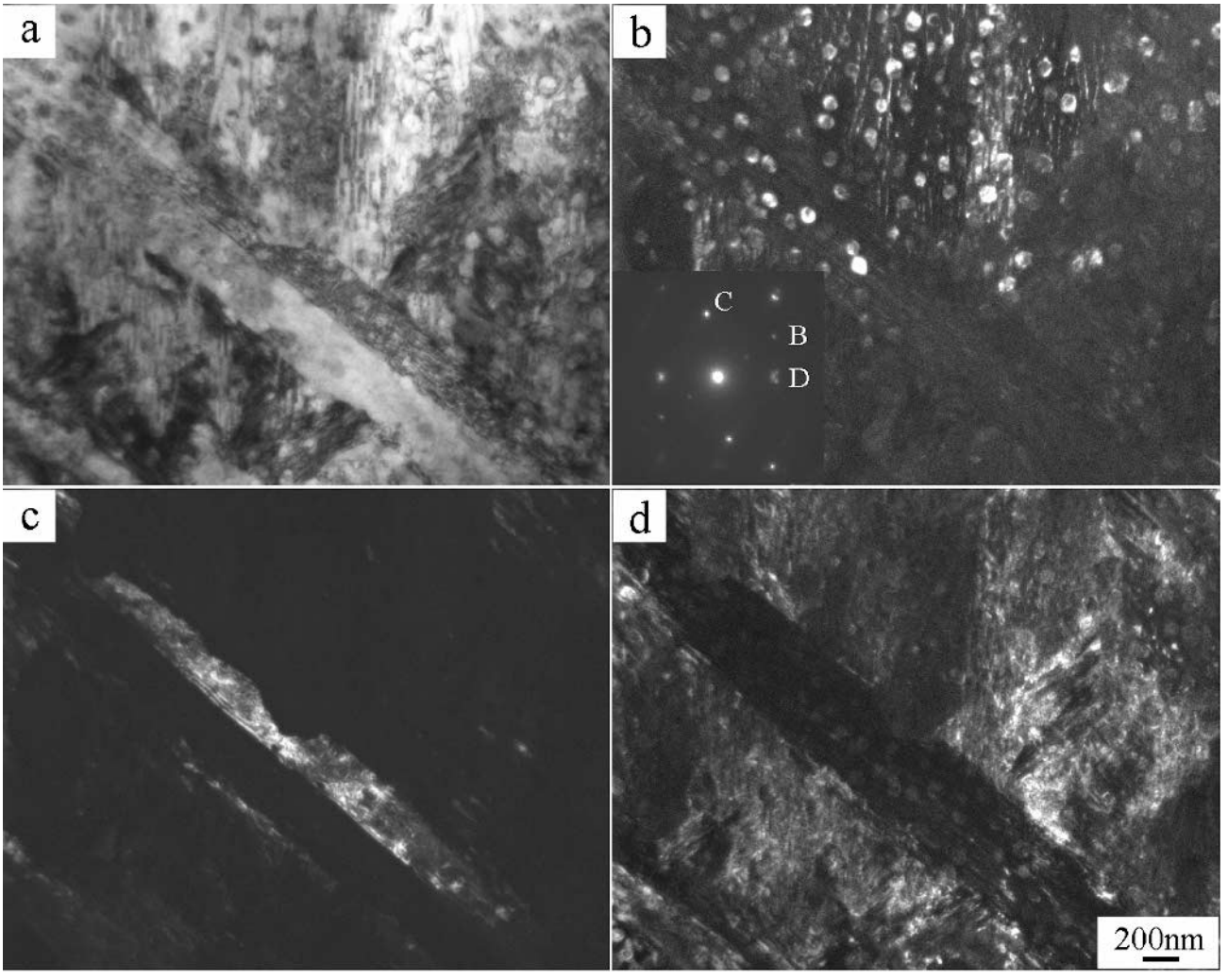

Fig. 6—TEM micrographs at a location toward the advancing side of the stir zone and near region 2 in Fig. 3 show an area of the bandlike structure that contains transformation products of the β phase. (*a*) The BF image, (*b*) through (*d*) The DF images taken using spots B, C, and D in the SAD pattern, respectively.

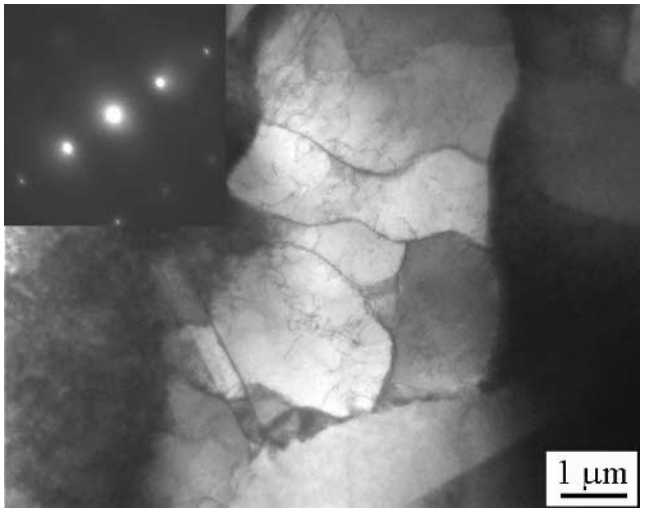

Fig. 7—A TEM micrograph illustrates the α phase in the bandlike structure in region 2. Substructure is apparent, and indicates occurrence of recrystallization, deformation, and recovery due to heating and severe deformation during processing.

removed from the surface. The α phase, with grains about 5 μm in size, was also observed in this foil. The α grains contained substructure and annealing twins, indicating that recovery and recrystallization occur simultaneously with phase transformations during the processing.

3. *Lower regions of the stir zone*

Figure 10 shows a TEM micrograph from region 4. In this location, the microstructure is highly refined and exhibits α grains about 2 μm in size. Particles of the various κ phases that have been broken up and partially spheroidized by the severe deformation are apparent along boundaries of the α grains and in between α grains in the structure. The rounded shape of these particles is indicative of the effect of the severe deformation when comparison is made to the as-cast NAB. The predominance of α and of deformation-induced changes in the κ phases likely reflects little or no β-phase formation due to lower peak temperatures in this region. In turn, this would account for the absence of a lamellar κ_{iii} phase that would form during subsequent cooling, as well as the absence of bainitic or martensitic transformation products. Incomplete transformation to martensite or a breakdown

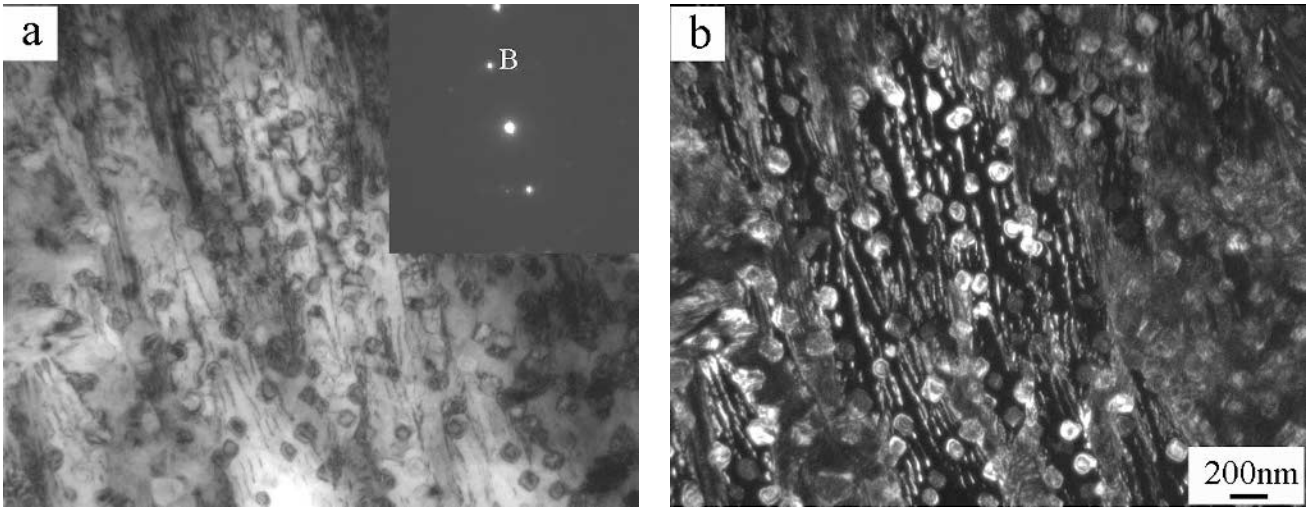

Fig. 8—TEM micrographs of region 3, near the middle of the stir zone, show fine and equiaxed α grains in this region. (*a*) The BF image, (*b*) The DF image taken using the spot B in the SAD pattern, showing fine lamellar-appearing and fine globular particles formed during cooling at a high rate.

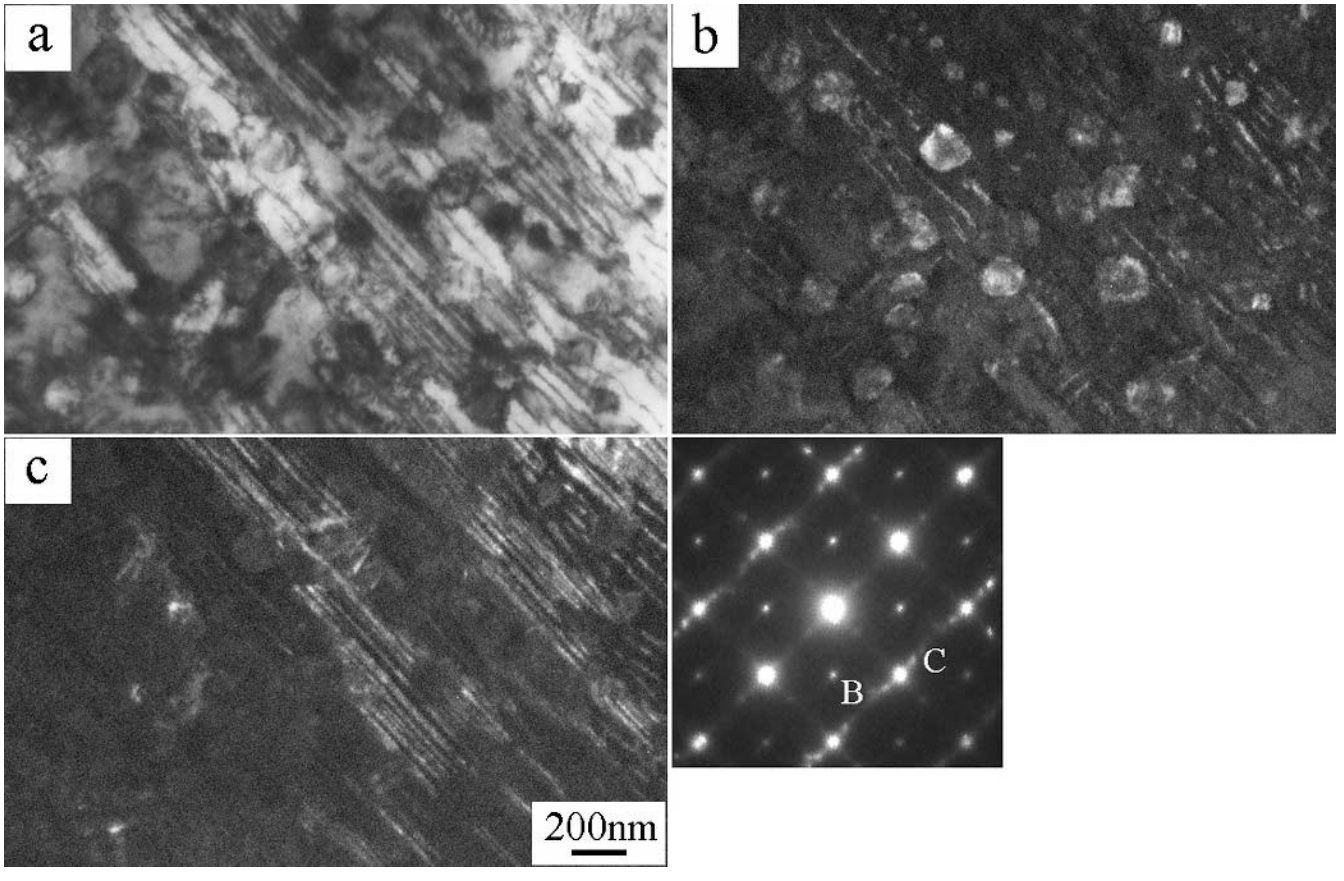

Fig. 9—TEM micrographs of region 3, near the middle of the stir zone, illustrate another location in the same sample of Fig. 8. (*a*) The BF image, (*b*) and (*c*) The DF images taken using spots B and C in the SAD pattern, respectively. A mixed structure consisting of bainite and martensite is apparent.

of the lamellar structure at moderate temperatures has been previously reported.[17]

Figure 11 is the microstructure at a location toward the advancing side of the stir zone nearby region 4. The grain size is 1 to 2 μm, which is the finest observed in the stir zone. The formation of annealing twins within the α grains is apparent. Fine particles about 100 nm in size are distributed along the grain boundaries of the α phase. In addition, there are clusters of irregularly shaped particles in the vicinity of grain triple points at several locations in Figure 11.

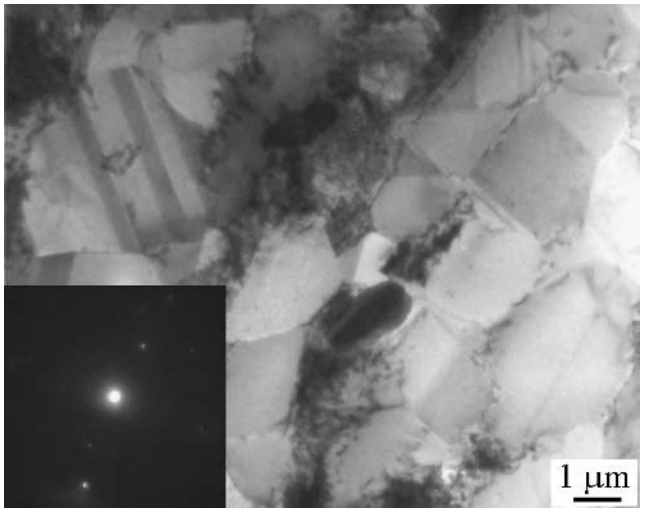

Fig. 10—A TEM micrograph of region 4, near the bottom center of the stir zone, shows a refined α grain structure with particles of the various κ phases that have been broken up and spheroidized by severe deformation.

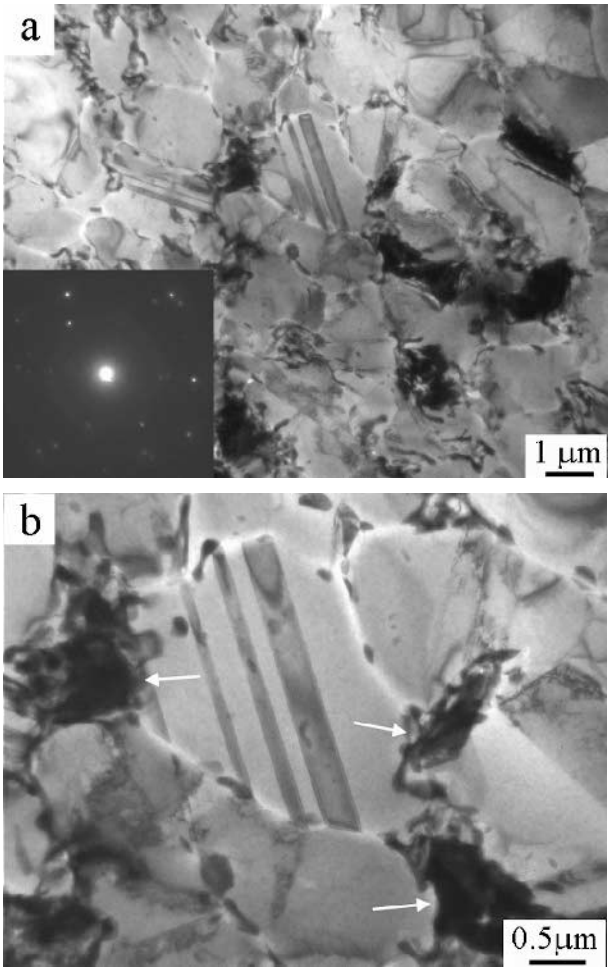

Fig. 11—TEM micrographs at a location toward the advancing side of the stir zone near region 4 show (*a*) the finest grain structure in the stir zone and (*b*) this same location at still higher magnification micrograph showing fine particles along the α boundaries as well as clusters of irregularly shaped particles in the vicinity of grain triple junctions (arrows). The formation of bainite and martensite is not evident in this region, suggesting a local peak temperature $\leq$800 °C.

These clusters of particles may be remnants of the $\alpha + \kappa_{iii}$ eutectoid constituent that has experienced severe deformation. Neither bainitic nor martensitic transformation products of the β phase were observed in this region.

IV. DISCUSSION

It is apparent that a single FSP pass dramatically alters the microstructure of the stir zone from that of the as-cast NAB material. Various constituents, such as bandlike features, very fine lamellar-appearing bainitic structures, martensite, and highly refined grain structures were observed at different locations, which indicates significant variation in the thermomechanical history from location to location in the stir zone. There have been few investigations into the influence of concurrent deformation on the kinetics of phase transformations to aid in interpretation of the microstructures of this work. Also, segregation of alloying elements in the slowly cooled, as-cast NAB material will lead to variation in microstructures and this is a potential complication as well. Nevertheless, the local peak temperatures attained during FSP may be estimated based on microstructures for material at various locations in the stir zone. Such estimates are useful because direct temperature measurement within the stir zone is infeasible.

No data have been reported on phase-transformation kinetics during deformation of NAB. However, concurrent deformation has been shown to accelerate the rate of spheroidization of pearlite in steels of eutectoid and hypereutectoid carbon content, as well as to refine the carbide particle and ferrite grain sizes in these materials.[29,30,31] Thus, pearlitic eutectoid carbon steels that required prolonged annealing to achieve a fully spheroidized condition during static annealing became completely spheroidized in a short time during concurrent deformation in torsion at 700 °C (0.55 T_M). This required straining in torsion to an equivalent strain of 4.6 at a strain rate of 0.024 s^{-1}, and, so, the spheroidization was complete in ~190 seconds.[29] Among various possible mechanisms, an acceleration of self-diffusion in bcc α-Fe due to excess vacancy production associated with the severe deformation was deemed responsible for the increased rate of spheroidization in these eutectoid steels. In order to support this explanation, data describing the effect of concurrent deformation on self-diffusion in α-Fe[32] were extrapolated to the torsion conditions employed with the steels. This extrapolation indicated that the self-diffusion coefficient in α-Fe would be increased by a factor of 2.5×10^4 due to excess vacancy generation, a factor sufficient to reduce the time for transformation by orders of magnitude.[29] The carbide particles and ferrite grains in the severely strained material were much finer than those produced by static annealing at this temperature. In ultrahigh-carbon steels (1.2 to 1.9 pct C), superplasticity was enabled by the production of grains 0.5 to 5 μm in size, stabilized by carbide particles 0.1 μm in size, during conventional rolling at temperatures just below the eutectoid.[30,31]

Static annealing of this as-cast NAB was conducted at temperatures of 770 °C to 1000 °C (0.78 to 0.95 T_M). Equilibrium microstructures were apparent within 1 hour of annealing at temperatures above 870 °C.[33] Increased diffusion rates due to excess vacancy production during FSP

would accelerate the reaction for the reversion of the lamellar $\alpha + \kappa_{iii} \rightarrow \beta$ upon heating into this temperature range, despite the lower overall diffusion rates in fcc α-Cu when compared to bcc materials in the same homologeous temperature range. Thus, it will be assumed in the following discussion that FSP-induced microstructure changes in the stir zone reflect local equilibrium upon attainment of peak temperature, so that the reverse of the reactions summarized in Figure 2 will occur on heating. The β phase formed by the reversion reaction $\alpha + \kappa_{iii} \rightarrow \beta$ is expected to experience deformation mainly at the peak temperature and then to cool to room temperature, where it is not stable. Typically, cooling rates encountered during FSP are greater by a factor of 10^3 than those encountered during casting of large components. Such cooling rates are evidently sufficient for the β phase formed during deformation at the local peak temperature to transform to Widmanstätten α, bainite, or martensite, despite refinement of the prior-β grain size relative to the as-cast material. These products of β decomposition are apparent as dark-etching areas in low-magnification OM, *e.g.*, as seen both within the stir zone and in the TMAZ beyond the stir zone/TMAZ boundary in Figure 3, or in Figure 4. At higher OM magnifications, the Widmanstätten α may be resolved as a lighter-etching constituent, *e.g.*, as in Figure 5(a) or the upper areas of Figure 5(b). The eutectoid reaction $\beta \rightarrow \alpha + \kappa_{iii}$ on cooling has been reported to occur at ~800 °C.[24] Therefore, the presence of β-phase decomposition products indicates that the local peak temperature exceeds this value during FSP.

Second, the relatively fine κ_{iv} precipitates will redissolve into the α phase upon attaining a peak temperature of 860 °C, but will also tend to reprecipitate upon cooling as still finer particles. Third, the relatively coarse κ_{ii} particles will likewise dissolve into the β phase as the local peak temperature exceeds 930 °C. Finally, for an NAB containing 9.4 wt pct Al, the fraction of β will increase with increasing temperature until ~1030 °C, whereupon a single-phase β solid solution will be present. In this investigation, the persistence of coarse κ_{ii} and the appearance of Widmanstätten α, bainite, and martensite as transformation products of β were especially useful in estimation of the local peak temperature in the stir zone. A montage of micrographs from the plate surface downward through the center of the stir zone to its boundary with the TMAZ and onward into base metal is provided in Figure 12 along with a corresponding estimate of the local peak temperature through this region.

The microstructure nearest the surface in contact with the tool, *e.g.*, region 1 in Figure 4, is apparently finer than that further below the surface. This reflects the severest straining in the stir zone due to friction with the tool shoulder as well as the tool pin. In Figure 5(a), the presence of relatively coarse Widmanstätten α along with other products of β decomposition in region 1 reveals that the peak temperature at the surface region is the highest in the stir zone despite the chilling effect of contact with the tool. On the other hand, the persistence of coarse κ_{ii} at all locations up to the surface indicates that the peak temperature does not exceed 930 °C. In the slowly cooled as-cast material, the κ_{ii} particles are coarse (typically ~20 μm in size), which reflects the high solvus temperature for this constituent (Figure 2). It is anticipated that during FSP, the κ_{ii} may require

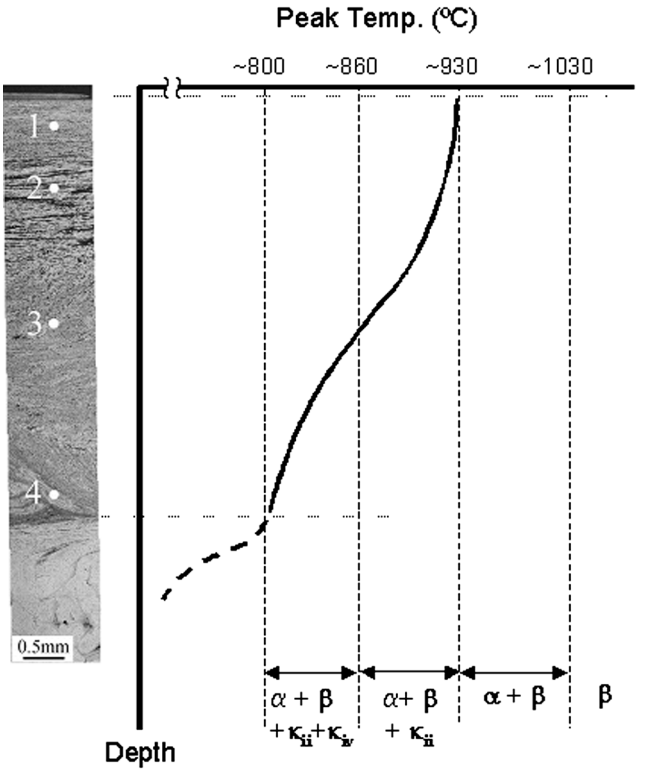

Fig. 12—A montage of micrographs summarizes the variation in microstructure through the center of the stir zone while the distribution of peak temperatures is plotted *vs* depth in the stir zone at the same scale. The estimated peak temperature values were determined by the relative amounts of various microstructure constituents and the transformation characteristics of the alloy.

more time and strain to revert to solution than the κ_{iv} particles or the lamellar $\alpha + \kappa_{iii}$ constituent, and this will introduce some uncertainty in estimates based only on the persistence of this phase.

Further below the surface, *i.e.*, region 2 in Figure 4, a bandlike structure is apparent; the light-etching features are α phase, while the dark-etching features comprise various transformation products of the β phase. Both features are elongated in a direction perpendicular to the tool axis. The lamellar $\alpha + \kappa_{iii}$ formed by eutectoid decomposition in regions that solidified last due to segregation of the Al. When the alloy is subsequently heated, the first major change in structure will be the reversion of the lamellar eutectoid structure to form β phase. The β will also contain κ_{ii} and will be surrounded by the remaining, untransformed α. When the peak temperature is in the $\alpha + \beta + \kappa_{ii}$ region and approximately equal volume fractions of α and β are present, severe deformation results in simultaneous deformation of both the α and β, and a bandlike structure is formed that is similar to those of two-phase alloys deformed by hot rolling or forging.

Outside of the stir zone in the TMAZ at locations under the tool shoulder, *i.e.*, to the side of the stir zone in Figure 3, the structure comprises a mixture of α and martensite that exhibits relatively small distortion at the stir zone/TMAZ boundary. Thus, the lamellar $\alpha + \kappa_{iii}$ structure has reverted to β phase in the TMAZ below the tool shoulder, and this appears to be the initial change upon approaching the stir zone from the base

metal. This supports the contention that the lamellar $\alpha + \kappa_{iii}$ constituent is the first to dissolve upon heating of the as-cast NAB. The appearance of martensite outside and on both sides of the stir zone just under the tool shoulder indicates that the temperature gradient in the vertical direction is steeper under the tool pin than under the tool shoulder.

Returning to the middle region of the stir zone, *i.e.*, region 3 in Figure 4, the α grains are fine and equiaxed, in contrast to the elongated α grains in region 2, and are the predominate constituent of the microstructure. Mixed structures comprising both bainite and martensite were also apparent in this region, but the bainite is refined and predominates in the mixed structure. Therefore, it is surmised that the peak temperature during FSP exceeds the eutectoid temperature but is lower than that in region 2, in which a larger proportion of β phase is apparent. In region 3, the severe deformation occurred in the presence of α, β, κ_{ii}, and κ_{iv}. The reversion of the lamellar $\alpha + \kappa_{iii}$ to β and the subsequent deformation results in the presence of the β transformation products along grain boundaries and at triple junctions in the α phase. The transformation to β will also occur at interfaces between the α and the κ_{ii}, because the κ_{iii} phase also tends to form on and surround coarse κ_{ii} particles during cooling after casting of the as-cast NAB. Furthermore, during heating, the κ_{iv} phase will first coarsen with increasing temperature, but then dissolve into the α phase above about 860 °C. In regions where the κ_{iv} has dissolved, the Fe and Al concentrations will be enriched, facilitating the local formation of β phase. Such a reaction at 860 °C is consistent with that reported by Culpan and Rose.[17] In addition to such transformations, severe deformation and heating during FSP will also result in recovery and recrystallization in the deforming α matrix as well as spheroidization of dispersed particles of remaining lamellar κ_{iii}.

Region 4, at the bottom of the stir zone, has the finest α grain size in the stir zone, as shown in Figure 11. From OM, there is little β present in this region, although the grain boundaries of the α grains are apparently decorated with particles of the κ_{iii} phase. Fine transformation products of β observed nearer to the surface are not evident in region 4, suggesting that the peak temperature is at or just over the eutectoid temperature, and the predominant effect is that of severe deformation by the FSP. This is also apparent in the presence of a large number of small particles produced by deformation and breaking of larger particles during the FSP. This, in turn, suggests that grain refinement may be by recrystallization due to particle-stimulated nucleation[34,35] in this region.

In conclusion, the distribution of peak temperatures during FSP of this NAB material may be estimated through analysis of the microstructures in the stir zone and TMAZ. The peak temperature is highest near the surface in contact with the tool, where the combination of transformation products of β phase and persistence of κ_{ii} suggests that it attains a value of ~930 °C. At the bottom of the stir zone immediately under the tool pin, the absence of β-phase transformation products and the presence of particulate κ phases due to deformation-induced refinement of second-phase particles is consistent with peak temperatures of ~800 °C. Extension of such analysis to consider other locations and different combinations of processing parameters will enable the development of predictive models of FSP.

V. CONCLUSIONS

Based on this study of the effect of FSP on the microstructure of a NAB material, the following conclusions are drawn.

1. The FSP of as-cast NAB materials provides microstructure refinement and homogenization as well as closure of porosity and improved mechanical properties.
2. In the present study, the presence and amount of κ_{ii} phase, as well as the relative amounts of products of β-phase decomposition, may be used to estimate the local peak temperature attained in the stir zone and TMAZ.
3. The presence of κ_{ii} particles throughout the stir zone indicates that $T_{Peak} \sim 930$ °C for the tool and processing parameters employed here.
4. Bandlike distributions of the α-phase and β-phase decomposition products in the stir zone near the plate surface reflect severe deformation (at 930 °C $> T_{Peak} >$ 850 °C) in the $\alpha + \beta$ region (of the phase diagram).
5. Highly refined, recrystallized grains 2 μm in size form at the bottom of the stir zone during the severe deformation of FSP at $T_{Peak} \approx 800$ °C.
6. Recrystallization associated with κ_{ii} and κ_{iv} particles as nucleation sites may account for refinement of as-cast grains.

ACKNOWLEDGMENTS

The authors acknowledge the provision of friction stir processed materials by Mr. Murray Mahoney, Rockwell Scientific Corporation. The Naval Surface Warfare Center (Carderock, MD) supplied the NAB material and the Defense Advanced Research Projects Agency (DARPA), with Dr. Leo Christodolou as program sponsor, provided funding for this work.

REFERENCES

1. R.S. Mishra: *Adv. Mater. Processes*, 2003, vol. 161 (10), pp. 43-46.
2. R.S. Mishra, Z.Y. Ma, and I. Charit: *Mater. Sci. Eng. A*, 2003, vol. A341, pp. 307-10.
3. Z.Y. Ma, R.S. Mishra, and M.W. Mahoney: in *Friction Stir Welding and Processing II*, K.V. Jata, M.W. Mahoney, R.S. Mishra, S.L. Semiatin, and T. Lienert, eds., TMS, Warrendale, PA, 2003, pp. 221-30.
4. W.M. Thomas, E.D. Nicholas, J.C. Needham, M.G. Murch, P. Templesmith and C.J. Daws: G.B. Patent Application No. 9125978.8, Dec. 1991; U.S. Patent No. 5460317, Oct. 1995.
5. R.S. Mishra and M.W. Mahoney: in *Superplasticity in Advanced Materials—Proc. ICSAM2000*, N. Chandra, ed., Materials Science Forum, Trans Tech Publications, Aedermannsdorf, Switzerland, 2001, vols. 357–359, pp. 507-14.
6. P.B. Berbon, W.H. Bingel, R.S. Mishra, C.C. Bampton, and M.W. Mahoney: *Scripta Mater.*, 2001, vol. 44, pp. 61-66.
7. R.S. Mishra, M.W. Mahoney, S.X. McFadden, N.A. Mara, and A.K. Mukherjee: *Scripta Mater.*, 2000, vol. 42, pp. 163-68.
8. I. Charit and R.S. Mishra: *Mater. Sci. Eng. A*, 2003, vol. A359, pp. 290-96.
9. Z.Y. Ma, R.S. Mishra, and M.W. Mahoney: *Acta Mater.*, 2002, vol. 50, pp. 4419-30.
10. Z.Y. Ma, R.S. Mishra M.W. Mahoney, and R. Grimes: *Mater. Sci. Eng. A*, 2003, vol. A351, pp. 148-53.
11. J.A. Duma: *Nav. Eng. J.*, 1975, vol. 87, pp. 45-64.
12. R.J. Ferrara and T.E. Caton: *Mater. Performance*, 1982, vol. 21, pp. 30-34.
13. E.A. Culpan and G. Rose: *Br. Corr. J.*, 1979, vol. 14, pp. 160-66.
14. G.M. Weston: *"Survey of Nickel-Aluminum Bronze Casting Alloys for Marine Applications,"* Australia Department of Defence Report DSTO MRL-R807, Melbourne, 1981.
15. P. Brezina: *Int. Met. Rev.*, 1982, vol. 27, pp. 77-120.

16. M. Hansen and K. Anderenko: *Constitution of Binary Alloys*, 2nd ed., McGraw-Hill, New York, NY, 1958, pp. 84-89.
17. E.A. Culpan and G. Rose: *J. Mater. Sci*., 1978, vol. 13, pp. 1647-57.
18. A. Cohen: *Metals Handbook*, 10th ed., ASM INTERNATIONAL, Metals Park, OH, 1990, vol. 2, pp. 386-87.
19. G.W. Lorimer, F. Hasan, J. Iqbal, and N. Ridley: *Br. Corr. J*., 1986, vol. 21, pp. 244-48.
20. D.M. Lloyd, G.W. Lorimer, and N. Ridley: *Met. Technol*., 1980, vol. 7, pp. 114-19.
21. F. Hasan, G.W. Lorimer, and N. Ridley: *Proc. Int. Conf. on Solid to Solid Phase Transformations*, TMS, Warrendale, PA, 1982, pp. 745-49.
22. F. Hasan, A. Jahanafrooz, G.W. Lorimer, and N. Ridley: *Metall. Trans. A*, 1982, vol. 13A, pp. 1337-45.
23. F. Hasan, G.W. Lorimer, and N. Ridley: *J. Phys*., 1982, vol. 43, pp. C4 653-58.
24. A. Jahanafrooz, F. Hasan, G.W. Lorimer, and N. Ridley: *Metall. Trans. A*, 1983, vol. 14A, pp. 1951-56.
25. F. Hasan, G.W. Lorimer, and N. Ridley: *Met. Sci*., 1983, vol. 17, pp. 289-95.
26. F. Hasan, J. Iqbal, and N. Ridley: *Mater. Sci. Technol*., 1985, vol. 1, pp. 312-15.
27. P. Weill-Couly and D. Arnaud: *Fonderie*, 1973, No. 322, pp. 123-35.
28. M.W. Mahoney: Rockwell Scientific Company, Thousand Oaks, CA, private communication, Dec. 2002.
29. J.L. Robbins, O.C. Shepard, and O.D. Sherby: *J. Iron Steel Inst*., 1964, vol. 202, pp. 804-07.
30. O.D. Sherby, B. Walser, C.M. Young, and E.M. Cady: *Scripta Metall*., 1975, vol. 9, pp. 569-74.
31. B. Walser and O.D. Sherby: *Metall. Trans. A*, 1979, vol. 10A, pp. 1461-71.
32. K. Hirano, M. Cohen, B.L. Averbach, and N. Ujiiye: *Trans. AIME*, 1963, vol. 227, pp. 950-57.
33. J. Sherburn: Naval Post Graduate School, Monterey, CA, private communication, Aug. 2003.
34. F.J. Humphreys: *Acta Metall*., 1977, vol. 25, pp. 1323-44.
35. R.D. Doherty, D.A. Hughes, F.J. Humphreys, J.J. Jonas, D. Juul-Jensen, M.E. Kassner, W.E. King, T.R. McNelley, H.J. McQueen, and A.D. Rollett: *Mater. Sci. Eng. A*, 1997, vol. A238, pp. 219-74.